Case Studies in Thermal Engineering 87 (2026) 108588

Contents lists available at ScienceDirect

Case Studies in Thermal Engineering

journal homepage: www.elsevier.com/locate/csite

Experimental characterization of a thermoelectric active insulation panel for boundary-matched thermal control

Minseong Kim, Junseok Park, Jae-Weon Jeong *

Department of Architectural Engineering, College of Engineering, Hanyang University, 222, Wangsimni-ro, Seongdong-gu, Seoul, 04763, South Korea

GRAPHICAL ABSTRACT

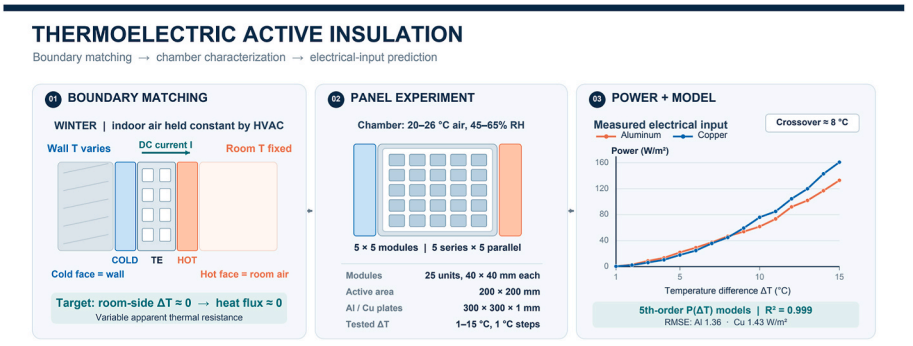

ARTICLE INFO

Keywords:
Thermoelectric technology
Active insulation
Dynamic thermal resistance
Boundary matching
Empirical model

ABSTRACT

This study presents an experimental evaluation of a thermoelectric active insulation panel proposed as a proof-of-concept building-envelope component for boundary-matched thermal control. Prototypes comprising a 5 × 5 array of thermoelectric modules bonded to aluminum or copper plates were evaluated in a controlled climate chamber at temperature differences (ΔT) of 1 to 15 °C. Electrical power consumption increased nonlinearly with ΔT, with relatively low electrical demand observed below approximately 9 °C under the tested conditions. This range represents a potential operating region for further energy-performance assessment rather than a verified net energy-saving regime. The aluminum prototype consumed more power at lower ΔT, whereas the copper prototype consumed more at higher ΔT, with a crossover near 8 °C; the underlying mechanisms require further verification. Fifth-order polynomial regressions reproduced the measured power consumption with R^2 values of approximately 0.999 and root mean square errors of 1.36 and 1.43 W/m^2 for the aluminum and copper prototypes, respectively. The results provide

* Corresponding author.
E-mail address: jjwarc@hanyang.ac.kr (J.-W. Jeong).

https://doi.org/10.1016/j.csite.2026.108588
Received 23 August 2026; Received in revised form 18 September 2026; Accepted 29 September 2026
Available online 1 October 2026
2214-157X/© 2026 The Authors. Published by Elsevier Ltd. This is an open access article under the CC BY-NC-ND license (http://creativecommons.org/licenses/by-nc-nd/4.0/).

Nomenclature

A	uniform cross-sectional area [m^2]
I	current [A]
L	thickness [m]
N	number of thermocouples [−]
P	electrical power [W]
Q	thermal capacity [W]
R	electrical resistance of thermoelectric module [Ω]
R^2	coefficient of determination [−]
T	temperature [°C]
V	voltage [V]

Greek symbols

Δ	difference [−]

Subscripts

c	cold side
h	hot side
max	maximum

Abbreviations

HVAC	heating, ventilation, and air conditioning
RMSE	root mean square error

electrical-input characteristics and empirical correlations within the tested configuration and boundary conditions. Direct heat-flux measurements, wall-assembly energy-balance assessment, and closed-loop control validation are required before confirming thermal benefits and whole-building energy savings.

1. Introduction

The building sector is a major contributor to global energy consumption and greenhouse gas emissions. Recent reports estimate that nearly 40% of worldwide primary energy use and more than one-third of the total emissions originate from this sector [1–3]. Most of this demand arises from heating and cooling, which makes the thermal performance of building envelopes crucial to both energy efficiency and climate policy. Conductive heat transfer through opaque wall assemblies continues to be the dominant source of energy loss and gain. This problem is particularly pronounced in regions with strong seasonal and substantial daily fluctuations. For these reasons, researchers and policymakers consistently highlight the improvement of building envelope performance as a necessary step toward nearly zero energy buildings and resilient construction practices [4–6].

For many decades, investigations have focused on passive insulation. Conventional materials, such as mineral wool, expanded polystyrene, and polyurethane foam, have long been used to provide static resistance to heat transfer. More advanced solutions, including silica aerogels and vacuum insulation panels, have enabled thinner assemblies with improved performance [7–9]. Despite these advances, passive insulation has a fundamental limitation: its resistance is fixed and cannot adapt to variable environmental conditions. As a result, passive layers do not actively prevent discomfort caused by radiant asymmetry, they do not eliminate the perception of cold walls in underinsulated interiors, and they do not reliably suppress condensation in humid climates [10–12]. Passive measures reduce conduction, but they cannot dynamically regulate it.

To address these shortcomings, researchers have explored different forms of active thermal control. Hydronic facade panels with embedded piping can raise or lower surface temperature to limit condensation and improve comfort [13,14]. However, such systems require pumps, valves, and hydraulic circuits, which increase the design complexity, create risks of leakage, and demand regular maintenance [15]. Air curtains and pressure-controlled vestibules have been applied at building openings to reduce convective exchange, but they do not mitigate conduction through opaque walls and may introduce drafts or noise [16]. Other facade systems that incorporate phase-change materials or ventilated cavities can buffer temperature and humidity fluctuations, although they lack continuous controllability [17–19]. In general, these active measures show promise but have not yet delivered a scalable or practical solution for substantially reducing conductive heat transfer through opaque walls.

Thermoelectric technology represents a different path. Based on the Peltier effect, first described in the 19th century, thermoelectric modules transfer heat when current is applied across semiconductors connected in electrical series and thermal parallel. One side becomes hot, while the other side becomes cold. Thermoelectric devices are compact, solid state, and do not require refrigerants. They have therefore been adopted in portable refrigerators, electronic component cooling, and local condensation management

[20–22]. However, their relatively low coefficient of performance compared with that of vapor compression machines restricts their application to small-scale or specialized uses [23,24].

In building science, thermoelectric devices have been tested in specific applications, such as radiant cooling panels [25,26] and surface treatments designed to prevent condensation [27]. These studies confirm technical feasibility but remain fragmented, limiting their scope to specific components rather than whole-building systems. No previous research has provided an experimental framework for evaluating thermoelectric modules as a continuous wall layer intended to suppress conductive heat transfer through opaque wall assemblies. Filling this gap may support the development of building-envelope technologies that move beyond conventional passive insulation toward electrically assisted thermal boundary management. The significance of this issue has become clearer in the wider context. Passive insulation has reduced U-values but cannot respond to transient or extreme events. Active methods, such as hydronic panels, ventilated facades, and air curtains, provide only partial control. The lack of an integrated solution forces designers to rely on increasing insulation thickness together with complex mechanical systems to meet stringent energy codes.

This paper introduces a thermoelectric active insulation panel as a proof-of-concept prototype rather than a fully validated active envelope control system. The system was designed as a prefabricated interior wall element that integrates an array of thermoelectric modules between two metallic conduction plates. These plates distribute the surface temperature and provide structural rigidity. In winter, the panel imposes a temperature difference (ΔT) by aligning the cold side with the outdoor-influenced substrate and the hot side with the indoor setpoint. In summer, the orientation is reversed so that the hot side faces outdoors while the cold side faces indoors. When the imposed ΔT approaches the boundary temperature difference, conductive exchange can be significantly suppressed, producing an apparent increase in effective thermal resistance under the assumed boundary-matching condition.

The implications extend beyond conductive heat-transfer suppression. By maintaining interior surfaces close to indoor setpoints, the panel may reduce radiant asymmetry and cold-wall discomfort, both of which are well-known causes of dissatisfaction in underinsulated buildings [28,29]. By keeping wall surfaces above the dew point, condensation and mold risk may be reduced under suitable operating conditions, which is difficult to achieve with passive insulation in humid or monsoon climates [30–32]. The panel also provides potential benefits to renovation projects. It can be installed as a single interior layer without major demolition or facade modification. This makes it particularly useful for older buildings with limited structural reserves or for situations constrained by cost, policy, or regulation [33,34].

The contributions of this study can be summarized in four points: First, thermoelectric modules are investigated as integrated building-envelope components rather than only as localized thermal devices, thereby extending their potential role toward active insulation concepts. Second, this work experimentally characterizes the electrical input required to maintain controlled ΔT conditions, providing prototype-level data beyond purely idealized assumptions. Third, it develops empirical predictive models for estimating panel power consumption within the tested operating range. Fourth, it identifies operating conditions under which conductive exchange may be substantially suppressed with moderate electrical input, thereby providing a basis for future building-scale validation.

The remainder of this paper is organized as follows. Section 2 explains the operating principle and design of the thermoelectric active insulation panel, with attention to its configuration, integration into walls, and installation. Section 3 describes the methodology, including the prototype fabrication with aluminum and copper plates, controlled chamber tests, model development, and uncertainty analysis. Section 4 presents the results, interprets the prototype performance, and evaluates regression accuracy. Section 5 concludes the paper by synthesizing the findings, clarifying the limitations of the present proof-of-concept study, and outlining opportunities for future validation and control development.

2. System description

2.1. Fundamental working principle of thermoelectric active insulation

Thermoelectric technology is based on the Peltier effect, which was first documented in 1834. This effect refers to the generation of a heat flux at the junction between two different conductive materials when an electric current flows through the circuit. Modern thermoelectric modules contain many n–p semiconductor couples that are connected electrically in series and thermally in parallel between two ceramic plates. When direct current is applied, one surface functions as the cold side while the other functions as the hot side. The maximum (ΔT) across the module is influenced by the magnitude of the applied current, intrinsic material properties (such as the Seebeck coefficient, electrical resistivity, and thermal conductivity), and boundary heat transfer conditions at the interfaces. Because thermoelectric modules are compact, solid state, and do not require refrigerants, they have been adopted mainly in small-scale applications. Examples include portable refrigerators, cooling of electronic components, and localized condensation management. Their relatively low coefficient of performance in comparison with vapor compression systems has restricted their adoption in large-scale heating, ventilation, and air conditioning (HVAC) systems. For this reason, applications in the building sector that exploit both the hot and cold sides in a coordinated manner remain rare and have not been thoroughly explored.

The thermoelectric active insulation panel reinterprets the purpose of thermoelectric modules by shifting their role from directly supplying heat or cooling to suppressing conductive heat transfer through opaque wall assemblies. Instead of transferring large quantities of heat into or out of occupied spaces, the panel applies electrical input to create and maintain a controlled ΔT across a thin wall-mounted layer. In this configuration, each surface of the panel is intended to follow the temperature of the adjacent boundary. During winter operation, the cold side is aligned with the substrate that is influenced by outdoor conditions, whereas the hot side is stabilized at the indoor comfort setpoint. When the applied ΔT approaches the indoor–outdoor gradient, net conductive exchange across the panel can be strongly reduced. This condition should be interpreted as an apparent increase in effective thermal resistance rather than as a literal elimination of heat transfer, because Joule heating, parasitic conduction, interfacial resistance, and internal heat

transfer within the thermoelectric modules remain present. During the summer, the operating mode is reversed. The hot side is oriented toward the exterior, and the cold side is oriented toward the interior, which can reduce inward heat flow from warm outdoor environments into cooled indoor spaces.

Fig. 1 presents the operating principle of the thermoelectric active insulation panel under both winter and summer boundary conditions. During winter operation, the cold side of the panel aligns with the exterior wall surface, which is governed by outdoor conditions, whereas the hot side is kept near the indoor comfort setpoint. In this state, the panel uses electrical input to impose a ΔT corresponding to the gradient between indoors and outdoors. This boundary-matching condition reduces conductive exchange across the assembly. In the schematic, the interruption of the temperature gradient line indicates substantial suppression of conductive heat transfer rather than complete elimination of all heat-transfer mechanisms. In the summer, this sequence is reversed. The hot side of the module is oriented toward the exterior, which is exposed to higher temperatures, whereas the cold side is stabilized near the conditioned indoor environment. The panel then applies ΔT in the opposite direction. Consequently, inward heat flow from the exterior toward the interior can be reduced. The figure therefore illustrates the concept of boundary matching, in which each surface of the panel follows the temperature of the adjacent domain. By doing so, the system provides effective suppression of conductive exchange through opaque wall assemblies under the assumed boundary conditions.

This boundary-matching mechanism clearly distinguishes the thermoelectric active insulation panel from conventional passive insulation. Passive materials provide a fixed level of thermal resistance, defined at the time of installation, that does not respond to short-term variations at the boundary. In contrast, the thermoelectric active insulation panel imposes an electrically controlled temperature difference across a thin layer. In principle, when the panel maintains the boundary-matching condition, conductive exchange through opaque walls can be substantially reduced. This concept does not imply infinite thermal resistance or complete removal of heat transfer. Rather, it indicates that the effective thermal behavior of the wall assembly can be modified by electrical input under defined operating conditions. The apparent increase in effective thermal resistance discussed here is a conceptual interpretation, not a measured resistance or U-value. Quantifying an equivalent thermal metric for the powered assembly requires direct heat-flux measurements with clearly defined boundaries, heat-flow direction, and operating conditions.

2.2. System configuration

The thermoelectric active insulation panel was designed as a prefabricated interior wall element that can be installed using procedures similar to those of conventional drywall construction. Each panel comprises two integrated layers. The first layer is an array of thermoelectric modules arranged in standardized grids, while the second layer is a set of metallic conduction plates, made of aluminum or copper, bonded to the module surfaces to spread heat and add structural rigidity. The metallic plates equalize the surface temperatures, reduce the occurrence of local hot and cold spots, and create an assembly strong enough for fastening. For building-scale applications, the use of large panels is required. Individual thermoelectric modules are relatively small, with typical dimensions of 40 mm × 40 mm. For future building-scale applications, the modules could be integrated into standardized panels, for example 1.2 m × 2.4 m, corresponding to common interior sheet sizes. Inside each panel, the modules are connected in networks that combine series and parallel circuits. This arrangement ensures compliance with the manufacturer's voltage and current limits while evenly distributing power and minimizing electrical losses. Such panels could incorporate plug-and-play connectors and identification features to support future zone-level operation in future building applications. The configuration and assembly strategy are illustrated in Fig. 2.

Panels are intended to be mounted on the interior side of opaque wall assemblies. When the wall-facing surface operates as the cold side, continuous contact with the substrate and sealed panel edges are assumed to prevent indoor air from entering the panel–wall interface. The concealed cold surface is therefore not intended to be directly exposed to humid indoor air. Detailed condensation and

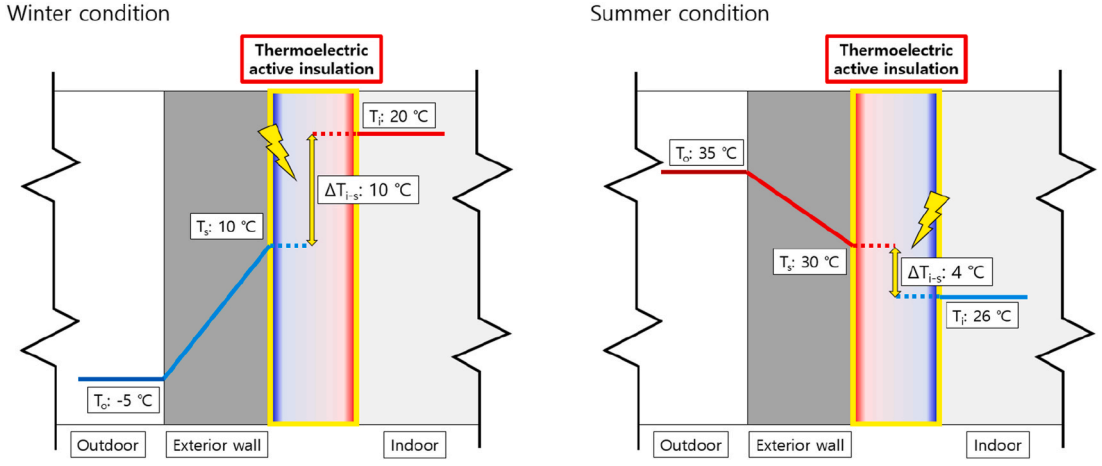

Fig. 1. Operating principle of thermoelectric panel.

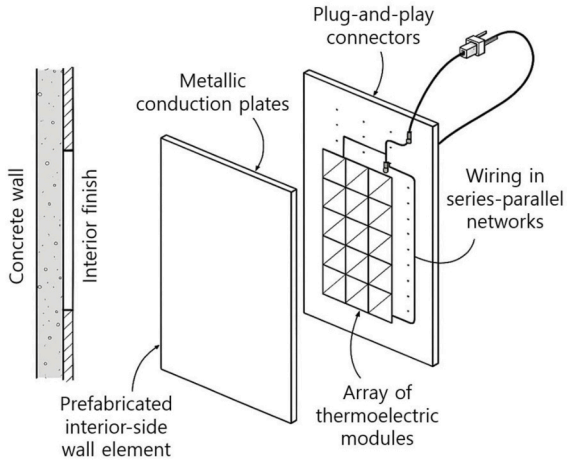

Fig. 2. Configuration and assembly of thermoelectric panel.

frost assessment depends on the wall assembly, substrate moisture, and installation details and is outside the scope of the present electrical-input characterization. This installation assumption does not exclude moisture transport through the wall; during reversed summer operation, the room-facing cold surface also requires consideration of indoor dew-point conditions.

Mechanical fixing and interior finishing should maintain the assumed thermal contact and sealed interface. For multi-panel installations, module spacing, interfacial thermal resistance, and thermal bridges at panel edges, fasteners, and supporting members require consideration. Spatially varying boundary conditions may also require zonal sensing and current regulation. These are building-integration considerations rather than experimentally validated features of the present prototype. The experiments were limited to controlled quasi-steady-state conditions; closed-loop control, transient response, and operational safeguards were not evaluated.

2.3. Building integration

At the scale of an entire building, the thermoelectric active insulation panel is conceived as a continuous interior layer that covers all opaque wall surfaces. In new construction, these panels can directly replace standard interior boards or be installed in their place without modifying the exterior facade or primary structure. This arrangement provides a potential route for electrically assisted boundary-temperature management in space-constrained applications. Its ability to reduce wall heat transfer or contribute to energy-code compliance requires wall-assembly validation.

In retrofitting projects, the benefits of the thermoelectric active insulation panel become even more evident. Many existing

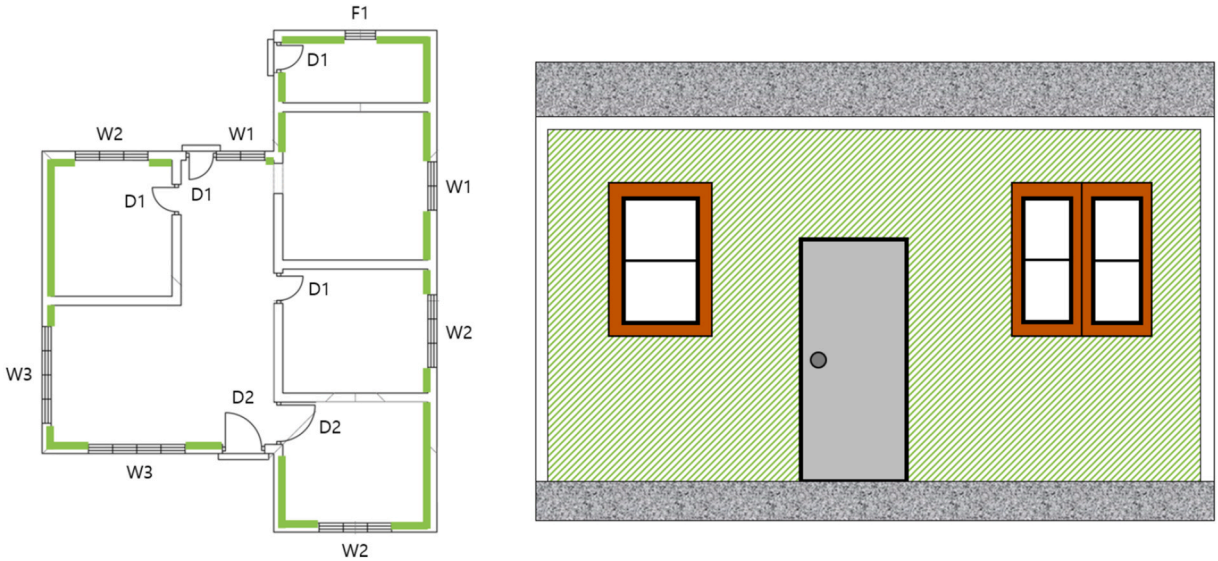

Fig. 3. Building integration of thermoelectric panels.

buildings show reduced insulation performance as a result of material degradation, moisture intrusion, or outdated construction practices. Conventional retrofits typically require the removal of interior finishes, installation of new insulation layers, or complete recladding of facades. Such methods are expensive, disruptive, and often limited by structural constraints. In contrast, the thermoelectric active insulation panel can be installed as a continuous interior layer with only minor demolition, thereby avoiding large interventions. The system can also be introduced gradually so that upgrades follow renovation schedules. This minimizes downtime, reduces inconvenience for occupants, and allows normal building functions to continue. Because the system is confined to the interior, exterior weatherproofing and architectural details remain untouched. This simplifies logistics and provides a realistic option for building types where traditional retrofitting would be technically or economically impractical.

Beyond reducing conductive heat transfer, the panel may also contribute to indoor environmental quality. By maintaining interior wall surfaces close to indoor setpoints, radiant asymmetry and cold-wall discomfort may be reduced. Likewise, maintaining wall surface temperatures above the indoor dew-point temperature may reduce condensation and mold risk under appropriate operating conditions. These potential benefits are inferred from the proposed operating principle and the measured thermal behavior of the prototype rather than from direct long-term building-scale measurements.

Fig. 3 depicts the building-level application of the thermoelectric active insulation panel. The figure on the left presents a representative floor plan. Green lines indicate the interior surfaces of the opaque perimeter walls where the panels are installed. Windows and doors are not marked because panels are not applied to these openings. The figure on the right shows the sectional interior elevation. Consistent with this plan, panels are applied to every interior surface of opaque walls that face outdoor conditions, while the fenestration remains untreated. Green hatching identifies wall areas covered by panels and distinguishes them from excluded openings. The schematic should be understood as a planning tool rather than a construction detail. The illustration is intended to demonstrate potential building integration only and does not represent a validated construction or control strategy. It demonstrates that the system can be integrated with typical layouts, preserve the exterior appearance, and allow phased retrofits so that some zones remain operational while others undergo upgrades.

2.4. Comparative performance and comfort advantages

Relative to passive insulation, which provides only static resistance defined by material properties and installed thickness, the thermoelectric active insulation panel introduces an electrically controlled thermal boundary condition. Under the proposed boundary-matching concept, conductive heat transfer through opaque wall assemblies can be substantially reduced without increasing insulation thickness. Unlike passive insulation, this approach allows the thermal boundary condition to be modified through electrical input. The present study experimentally characterizes this concept under controlled quasi-steady-state conditions rather than validating a complete active building-envelope control system.

Compared with advanced passive materials such as aerogels or vacuum insulation panels, the proposed system offers a fundamentally different operating principle because conductive heat transfer is modified through electrically imposed boundary conditions rather than solely through material resistance. Potential future implementations could include zonal operation, scheduled operation, and integration with building automation systems. However, these control functions were not experimentally investigated in the present study and therefore remain future development opportunities rather than validated capabilities.

Hydronic barriers and embedded coil systems require fluid piping networks, pumps, and extensive installation. In contrast, the proposed thermoelectric active insulation panel is a solid-state concept that does not require refrigerants or circulating fluids. Potential comfort benefits include more uniform interior surface temperatures and reduced cold-wall discomfort. However, these effects were not directly quantified in occupant-based experiments and are discussed here as expected implications of the proposed operating principle.

Earlier thermoelectric applications in buildings were limited to small cooling units or local condensation prevention. The thermoelectric active insulation panel is distinctive because it synchronizes the hot and cold sides of the modules with the indoor and outdoor boundaries across the entire opaque envelope. This study extends previous thermoelectric building applications by experimentally evaluating a prototype intended for potential building-scale implementation.

One important outcome of the present study is the identification of operating conditions under which the measured electrical input remains relatively low while conductive heat transfer is expected to be substantially reduced according to the proposed boundary-matching concept. Under these conditions, the reduction in HVAC demand may exceed the electrical power consumed by the thermoelectric panel. Because direct heat-flux measurements and whole-building energy-balance experiments were outside the scope of the present work, this potential net energy-saving behavior should be interpreted as a conceptual implication supported by the experimental electrical-input characteristics rather than as a directly validated building-energy result.

When the indoor–outdoor temperature difference remains within the low to moderate range, the panel can maintain the interior surface temperature close to the indoor set point, thereby reducing the temperature gradient across the wall assembly. This reduction in surface temperature difference is expected to suppress conductive heat transfer through opaque walls. As a result, heat loss during heating periods and heat gain during cooling periods may decrease, potentially reducing the thermal load that must be met by the HVAC system.

Although thermoelectric modules require electrical input to transport heat via the Peltier effect, the system is not intended to move large quantities of heat. Instead, it maintains boundary temperature alignment by sustaining a small controlled temperature difference across a thin layer. Under these conditions, the required heat pumping capacity remains limited, and the thermoelectric modules can operate with relatively low electrical input. The experimental results showed that when ΔT is below approximately 9 °C, the measured panel power consumption remains relatively low. When interpreted together with the proposed boundary-matching concept, this

result suggests a potential operating region in which the expected reduction in heating or cooling demand may exceed the panel's power consumption. However, this should be regarded as a conceptual implication rather than a directly verified net energy-saving result, because direct heat-flux measurements and closed whole-building energy-balance validation were not conducted in the present study.

As conceptually illustrated in Fig. 4, the expected HVAC load reduction can be represented as a positive contribution, while the measured panel electrical input can be represented as an energy cost across increasing ΔT. The shaded region indicates a potential operating range in which the expected load reduction may exceed the measured panel input. This figure is intended as a conceptual energy-performance framework based on experimentally measured electrical input and theoretical load-reduction interpretation. It should not be interpreted as direct experimental verification of whole-building net energy savings. A quantitative net-energy assessment must convert avoided thermal loads to avoided HVAC energy use using the relevant system efficiency and consistent area and time bases. Neither the shaded region nor the reference to approximately 9 °C establishes a measured energy-saving crossover.

Operational efficiency may be further enhanced through future control strategies. Output could be reduced under high ΔT conditions to avoid disproportionate increases in electrical consumption, while priority operation could be assigned to conditions within the relatively low-electrical-input range. In addition, future coordination with periods of renewable electricity availability or low-carbon grid intensity may improve primary energy and emissions performance. These possibilities were not experimentally validated in the present study. Therefore, the thermoelectric active insulation panel should be viewed as a proof-of-concept active envelope strategy intended to modify conductive heat transfer, while confirmation of HVAC demand reduction and net building energy savings requires direct heat-flux measurements and closed energy-balance validation.

Second, in terms of comfort and moisture control, the system may maintain interior wall surfaces close to indoor setpoints and above the dew point under suitable operating conditions. As a result, it may reduce cold-wall discomfort and lower condensation and mold risks. Passive strategies rarely guarantee these outcomes, particularly in humid or otherwise demanding climates. Third, the proposed system suggests potential operational flexibility. Unlike static insulation layers, the thermoelectric active insulation panel may be switched, scheduled, or assigned to selected zones in future building applications. These control functions were not experimentally validated in the present study. Fourth, the system suggests retrofit feasibility. Installation requires only a single interior layer with limited demolition, whereas the external facade remains untouched. This approach allows phased upgrades on a room-by-room basis and minimizes disruption to occupants. Table 1 summarizes qualitative differences between the thermoelectric active insulation panel and conventional passive insulation, advanced passive products, hydronic or coil-based systems, air curtain strategies, and previous thermoelectric applications.

Taken together, these comparisons indicate that the thermoelectric active insulation panel represents a conceptually different approach from existing passive and active insulation strategies. The prototype demonstrates the feasibility of electrically modifying thermal boundary conditions under controlled laboratory conditions. However, several anticipated advantages, including whole-building energy performance, long-term operational stability, advanced control capability, and occupant comfort improvements, remain topics for future investigation and should not be interpreted as experimentally validated outcomes of the present study.

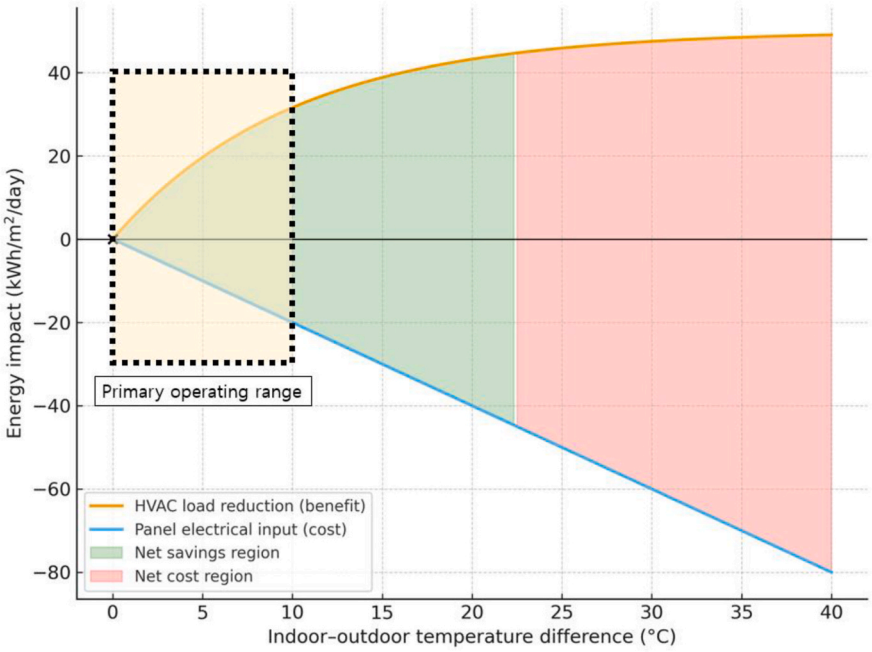

Fig. 4. Conceptual comparison of expected load reduction and measured panel input across temperature differences.

Table 1
Comparative analysis of insulation strategies.

Criterion	Conventional passive insulation	Advanced passive materials (aerogel, VIP)	Hydronic/coil-based active barriers	Air curtains & pressure zoning	Prior thermoelectric applications	Thermoelectric active insulation panel
Mechanism of action	Static thermal resistance	Static thermal resistance, very high	Active surface tempering via fluid circulation	Convective exchange reduction at openings	Localized spot cooling or condensation prevention	Active boundary matching across opaque envelope
Thickness/ weight	Medium to very thick, heavy	Thin but fragile, costly	Medium thickness, wet trades required	No thickness, relies on airflow	Device-scale only	Thin, lightweight, panelized
Controllability	None	None	Limited (valves, pumps)	On/off operation only	Device-level control	Potentially controllable (switchable and schedulable in future applications)
Responsiveness	None	None	Slow, due to fluid inertia	Fast, but limited to openings	Fast, but highly localized	Fast, solid-state response
Comfort impact	Reduces conduction, but cold walls remain	High-performance insulation, but static	Can improve surface temperature, uneven distribution	Drafts and acoustic issues	Spot comfort only	May reduce cold-wall effects and radiant asymmetry
Condensation control	Limited	Limited	Risk near coils if uneven	None	Spot dehumidification only	Maintains surfaces above dew point, suppresses mold
Retrofit complexity	High (demolition required)	Very high (cost, detailing)	Very high (piping, pumps, manifolds)	Moderate, but limited scope	Device installation only	Low (single interior layer, minimal demolition)
Impact on facade	Requires recladding or thick build-ups	Requires careful detailing, potential alteration	Requires penetrations, potential alteration	None	None	None (external appearance untouched)
Maintenance profile	Very low	Low to medium (fragile)	High (pumps, leaks, balancing)	Medium (fans, energy use)	Medium (device maintenance)	Low (modular, plug-and-play panels)
Typical use cases	New construction, low-cost retrofits	Space-constrained retrofits, high performance	Specialized projects, radiant conditioning	Entrances, lobbies	Niche condensation control	Broad new-build and retrofit applications

Note: This comparison summarizes general design considerations rather than results from matched wall-assembly tests. The proposed panel's comfort, moisture-control, transient-response, installation, and maintenance attributes remain conditional on implementation and have not been validated at building scale.

3. Experiment overview

3.1. Prototype model configuration

Two prototype models were produced for experimental evaluation, as illustrated in Fig. 5. The specifications of the thermoelectric modules used in these prototypes are presented in Table 2, with each model containing 25 modules. A previous study [35] has noted that when many thermoelectric modules are combined into a single system, the electrical configuration must be designed with attention to the rated voltage and current limits specified by the manufacturer. Stable operation is most likely when the balance between series and parallel connections is maintained close to unity, because this arrangement distributes the electrical load evenly and reduces the risk of localized overheating of individual modules. In this investigation, each prototype was designed with five thermoelectric modules connected in series to form a single unit. Five of these units were then connected in parallel to the main circuit, producing a five-series by five-parallel arrangement, as shown in Fig. 6. This configuration satisfies electrical safety requirements and simultaneously allows scalability for larger assemblies in building-scale applications. As a result, the prototypes provided a reliable platform for evaluating the electrical and thermal characteristics of the proposed proof-of-concept system under controlled laboratory conditions.

To achieve uniform surface temperature across the cold and hot sides, prevent structural warping, and enable practical integration into building envelopes, metallic plates with both high thermal conductivity and mechanical rigidity were bonded to the opposing surfaces of the thermoelectric array. Aluminum and copper were selected for this role. A previous study [13] showed that vertically oriented plates with a thickness of at least 1 mm provide adequate structural stability, while horizontally oriented plates require a thickness of 3 mm or more to avoid deformation under repeated thermal cycling. From both economic and thermal engineering perspectives, thinner plates are desirable. They lower material costs and reduce thermal resistance at the interface between the modules and plates, thereby improving heat transfer efficiency. For this reason, this study adopted aluminum and copper plates with a thickness of 1 mm as the design condition. In the fabricated prototypes, aluminum plates were attached to the wall-facing surface, while copper plates were attached to the air-exposed surface. This arrangement enabled a direct comparison of the two materials, allowing analysis of energy consumption patterns and assessment of how material selection influences the overall performance of the system.

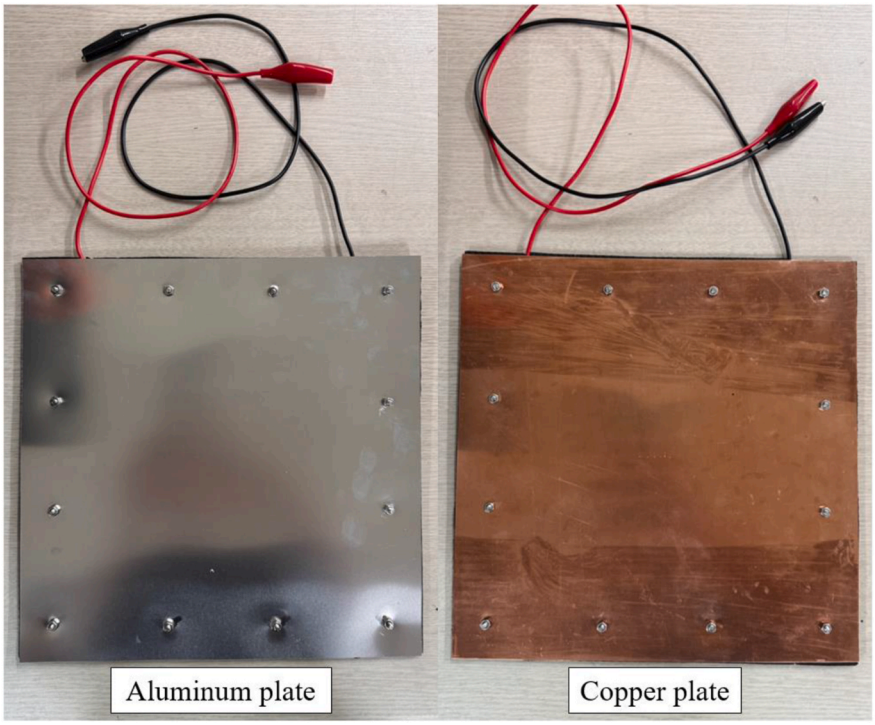

Fig. 5. Prototype thermoelectric insulation panels.

Table 2
Specifications of thermoelectric module.

Symbol	Description	Value
A	Dimension	40 mm × 40 mm
L	Thickness	3.9 mm
N	Number of thermoelement couples	127
ΔT_{max}	Maximum temperature difference	66 °C
$V_{\max}$	Maximum input voltage	14.4 V
$I_{\max}$	Maximum input current	6.4 A
$Q_{c,max}$	Maximum cooling capacity	50 W
R	Electrical resistance	1.98–2.30 Ω

The internal structure of the plates is depicted in Fig. 7. Each thermoelectric module had dimensions of 40 mm × 40 mm, and the modules were arranged in a 5 × 5 grid. This yielded an active surface area of approximately 200 mm × 200 mm. To ensure fastening strength and robust assembly, metallic plates with dimensions of 300 mm × 300 mm were bonded to both sides of the array, which provided sufficient allowance for bolt and nut compression. This fastening strategy was chosen to secure strong mechanical contact while minimizing interfacial thermal resistance. A high-conductivity thermal paste was also applied between the modules and plates to enhance coupling, reduce local hotspots, and improve thermal diffusion across the surface. To limit parasitic conduction through inactive areas, rubber foam insulation was applied around the periphery of the active zone. As a result, the effective measurement area was restricted to the 200 mm × 200 mm active region defined by the module array, as indicated by the yellow dashed line in Fig. 7. This ensured that the recorded data accurately represented the thermal and electrical behaviors of the modules without interference from external heat losses.

3.2. Experimental setup

The experiments were conducted under controlled laboratory conditions to ensure reproducibility and approximate the behavior of real building environments. All tests were conducted in a climatic chamber with controlled temperature and humidity, as shown in Fig. 8. The indoor side temperature, which represented the conditioned zone, was maintained within the thermal comfort range of 20–26 °C, in accordance with ASHRAE Standard 55 [36]. The relative humidity was regulated between 45% and 65% so that its effect on heat transfer would remain limited. The wall surface temperature, which represented the outdoor boundary condition, was imposed using a constant-temperature controller (Peltier plate, PTC, South Korea). The effective measurement area of the prototype was

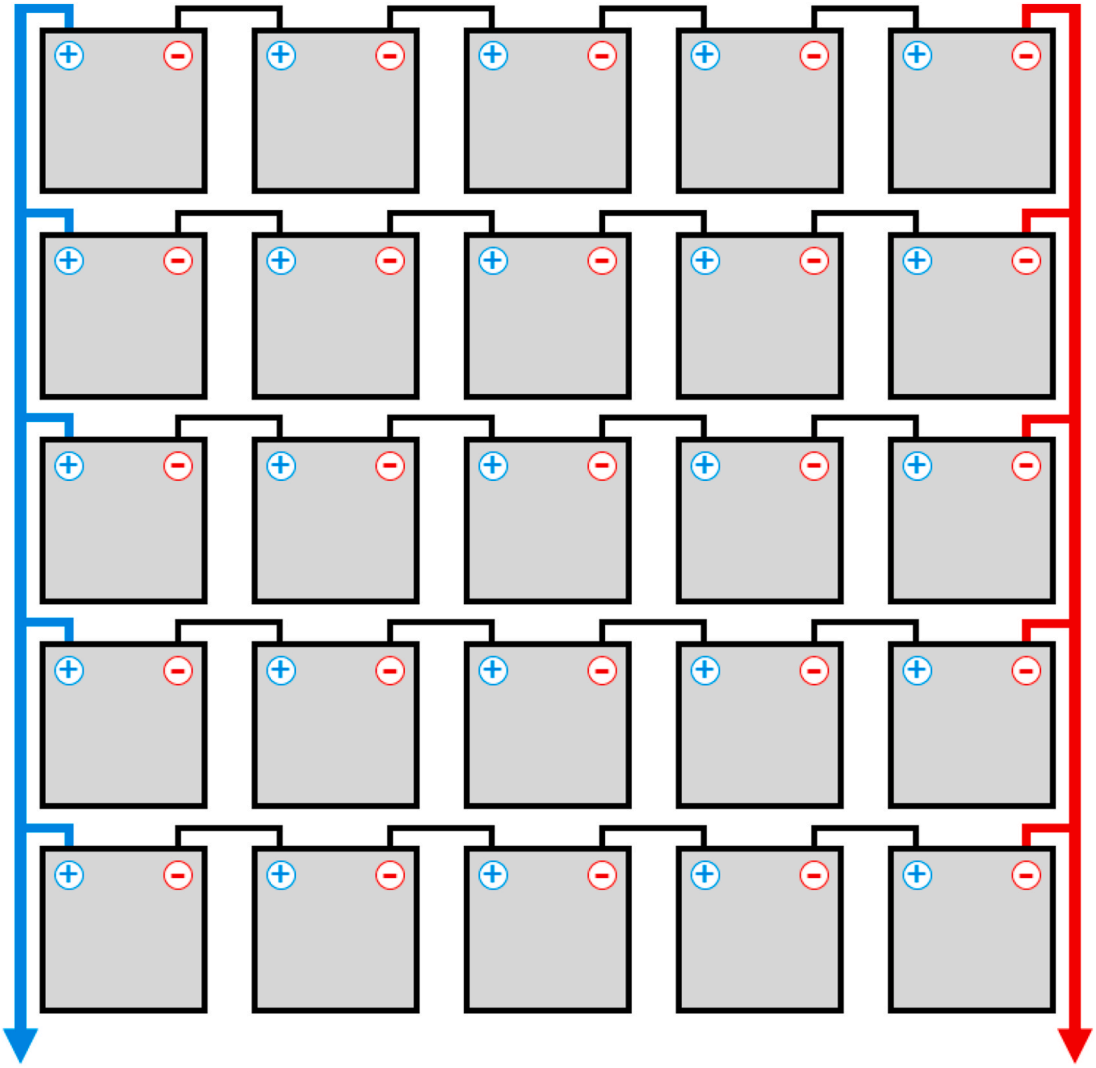

Fig. 6. Electrical circuit of prototype panel.

defined as the central 200 mm × 200 mm region of the thermoelectric array, as shown in Fig. 7. To reduce undesired heat transfer and interfacial resistance between the active insulation panel and Peltier plate, a thermal pad of high conductivity with dimensions of 200 mm × 200 mm was placed between them. Consequently, the performance evaluation was confined exclusively to the heat transfer occurring through the active module region. Accordingly, the experiments focused on prototype-level thermal characterization rather than validation of whole-building energy performance or closed-loop control.

The measurement system was arranged to capture the thermal and electrical responses simultaneously, as displayed in Fig. 9. Ambient air temperature and relative humidity in the vicinity of the thermoelectric active insulation panel were measured with a smart probe sensor (605i, accuracy ±0.5 °C and ±1.8% RH, Testo, Germany). Surface temperatures were obtained using T-type thermocouples (TT-T-30-SLE, accuracy ±0.5 °C, Omega, United States) attached at representative positions. Electrical input variables, including voltage and current, were provided and monitored with a switched-mode power supply. All measurements were recorded at 1-s intervals with a data logger (GL840, accuracy ±0.5 °C, operating range −200 to 400 °C, GRAPHTEC, Japan). The experimental program was designed to obtain quasi-steady-state electrical input characteristics under prescribed temperature differences rather than to evaluate transient control performance. To ensure reliable data, each run was continued until steady conditions were achieved. Saturation was defined as temperature variation smaller than 0.5 °C maintained for a minimum of 10 min.

3.3. Experimental cases

The energy consumption of a thermoelectric active insulation system is defined as the electrical input required to sustain the ΔT between the cold and hot sides through the Peltier effect. In the configuration used in this study, the cold side was thermally coupled to

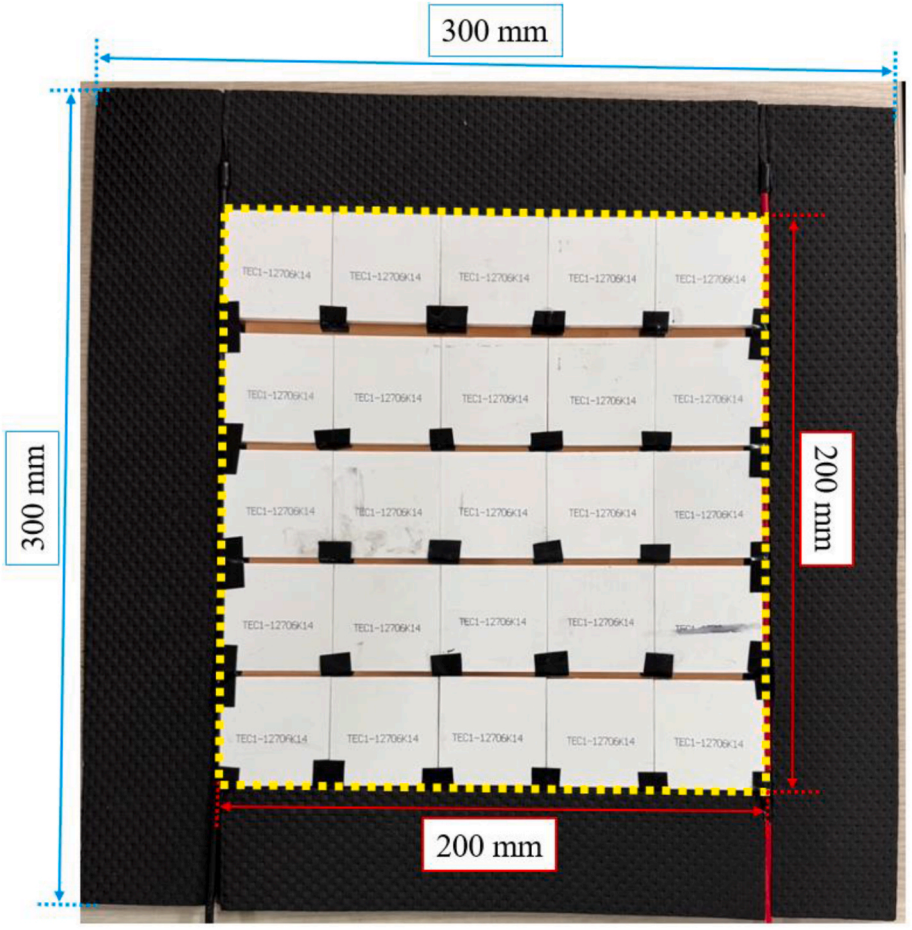

Fig. 7. Internal configuration of prototype panel.



Fig. 8. Climatic chamber for experiments.

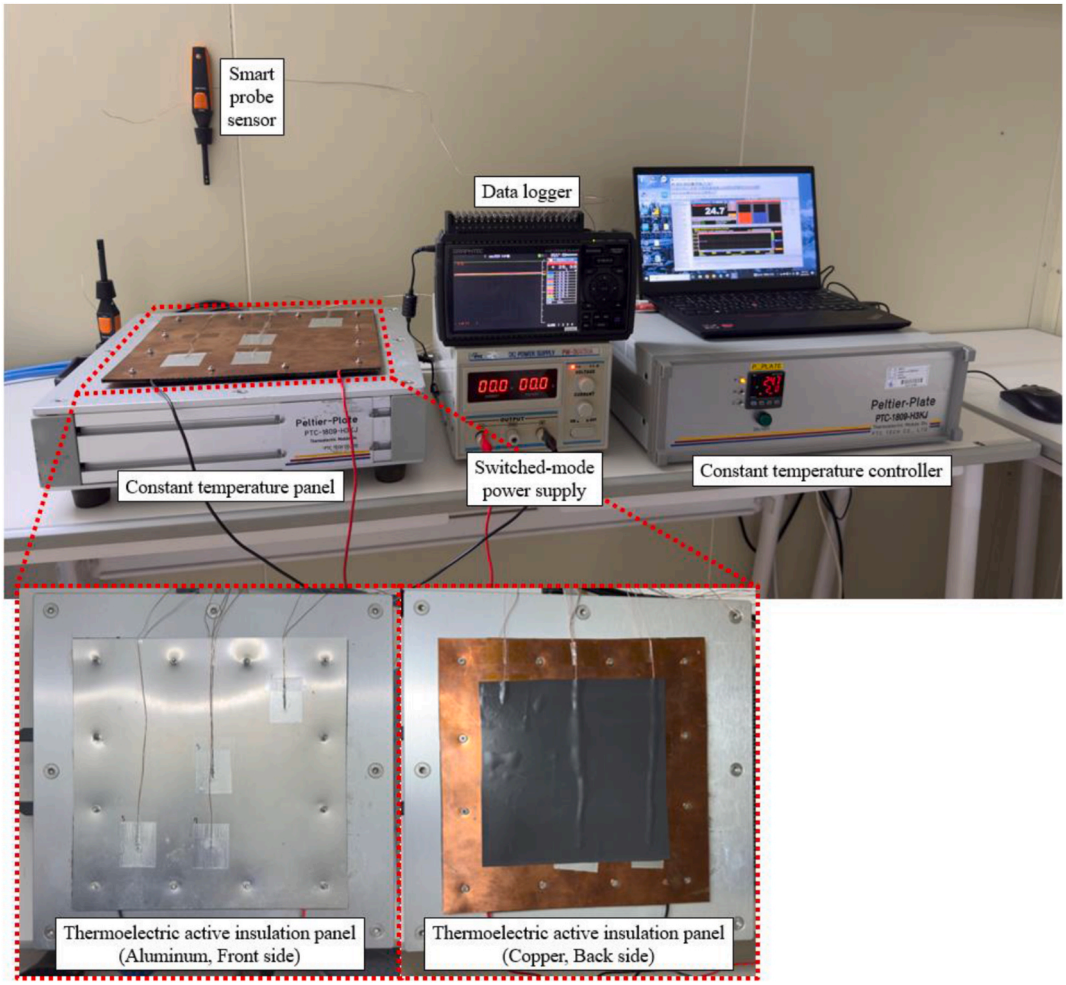

Fig. 9. Experimental setup.

the wall surface, whereas the hot side was coupled to the indoor air. As a result, the hot side operated within the indoor comfort range of 20–26 °C, consistent with ASHRAE Standard 55 [36]. This ensured that the experiments represented realistic boundary conditions and complied with human comfort requirements. Kim et al. [37], who applied annual climate datasets of South Korea to steady-state heat transfer analysis, reported that the cold side temperature can reach a minimum of 12.6 °C in winter and a maximum of 31.8 °C in summer. From these values, the maximum ΔT across the panel was calculated as 7.4 °C in winter and 5.8 °C in summer. These ΔT values are critical because they directly determine the electrical load imposed on the thermoelectric modules. This relationship provides the theoretical basis for defining operational limits and estimating seasonal performance profiles.

According to the manufacturer's specification sheet [38], electrical characteristics including internal resistance and the Seebeck coefficient remain nearly constant when the hot side is maintained near 25 °C, with only minor variations. The calibration results in Table 3 show the same reported electrical input at a given ΔT for the limited absolute-temperature conditions examined. Together with the related observations reported by Kim and Jeong [39], these results support using ΔT as the predictor for the present empirical correlations. They do not establish independence from absolute temperature under other operating conditions. Application to different

Table 3
Calibration experiment results.

T_c	T_h	ΔT	I	V	P
16 °C	20 °C	4 °C	0.7 A	2.5 V	1.75 W
18 °C	22 °C		0.7 A	2.5 V	
20 °C	24 °C		0.7 A	2.5 V	
18 °C	20 °C	2 °C	0.3 A	1.2 V	0.36 W
20 °C	22 °C		0.3 A	1.2 V	
22 °C	24 °C		0.3 A	1.2 V	

panel configurations or boundary conditions requires additional validation and, where necessary, recalibration.

The experimental cases in this study were organized into systematic categories, as listed in Table 4, to quantify the electrical energy consumption of the thermoelectric active insulation system as a function of ΔT between the hot and cold sides. This classification provides a structured basis for assessing performance and establishes a standardized framework for comparing thermoelectric insulation with conventional passive insulation in terms of energy efficiency, feasibility of operation, and cost effectiveness. To construct a model applicable not only to Korean climatic conditions but also to extreme cold and hot environments, the experimental program was designed to include a wide range of ΔT values. Tests were carried out from 1 °C to 15 °C in increments of 1 °C. The selected ΔT range was intended to characterize the operating behavior of the prototype within conditions considered representative of practical building-envelope applications. Two prototype panels were evaluated, one equipped with aluminum plates and the other with copper plates, under identical ΔT conditions. This allowed a direct comparison of the performance differences arising from the choice of metallic material. Although a detailed uncertainty analysis is presented separately in Section 4.3, the experimental program incorporated repeated measurements, sensor calibration, and statistical processing throughout the tests to ensure reliability. This methodology establishes a solid foundation for evaluating the performance of thermoelectric active insulation panels and for benchmarking them against conventional insulation systems.

4. Experimental results and discussions

4.1. Electrical energy consumption of thermoelectric active insulation

Fig. 10 presents the electrical power consumption of the aluminum and copper prototypes under the tested ΔT conditions. Electrical input was small at low ΔT, particularly below 3 °C, and increased more rapidly at larger temperature differences. The increase was approximately linear over the intermediate range and became steeper above approximately 10 °C. This behavior can be interpreted through the combined effects of Peltier heat pumping, Joule heating, and conductive backflow. In a simplified thermoelectric description with fixed effective properties, the Peltier term is proportional to current, Joule heating is proportional to the square of current, and conductive backflow depends on ΔT. Increasing the current required to sustain a larger ΔT can therefore increase electrical demand disproportionately. These contributions were not independently quantified, so the interpretation does not establish a unique physical threshold at 9 °C. The reference to approximately 9 °C describes a relatively low-input region of the tested prototypes, not a verified net energy-saving range. Such savings require an assessment of avoided thermal loads and HVAC energy use on consistent area and time bases.

The aluminum-based prototype consumed more electrical power at lower ΔT, whereas the copper-based prototype required more power at higher ΔT, with a crossover near 8 °C. Differences in lateral heat spreading, interface conditions, and parasitic heat-transfer paths may contribute to this behavior. However, the present measurements do not separate these contributions, and higher plate conductivity alone does not establish increased hot-to-cold heat leakage. The observed crossover is therefore distinguished from its tentative mechanistic interpretation. Because plate thickness was fixed at 1 mm and module spacing was not systematically varied, the present comparison does not identify an optimal plate conductivity or thickness. Detailed temperature mapping or a validated thermal model would be needed for such optimization.

Overall, the measurements show relatively low electrical demand in the low-to-moderate ΔT range, particularly below approximately 9 °C under the tested conditions. In this zone, the measured electrical input remains relatively low, indicating a favorable operating range for potential energy-saving applications under the proposed boundary-matching concept. Whether the corresponding heating or cooling load reduction exceeds the panel electricity consumption should be verified in future studies through direct heat-flux measurements and closed energy-balance analysis. When ΔT rises beyond this range, consumption increases sharply and imposes limits on performance. The observed crossover between the aluminum and copper panels further indicates that material properties strongly influence the behavior and must be regarded as a crucial design parameter in building applications.

4.2. Empirical models for predicting energy consumption

To enable reliable prediction of electrical power consumption across a wide range of operating conditions, empirical regression models were developed using the measured datasets obtained from the aluminum and copper thermoelectric active insulation panels. As discussed in Section 4.1, the power consumption exhibited pronounced nonlinear behavior with increasing ΔT; therefore, polynomial regression was adopted. Polynomial models from first-to sixth-order were evaluated. Models up to the fourth order showed insufficient accuracy, particularly in reproducing the curvature of the experimental data and the rapid increase observed at higher ΔT. In contrast, sixth-order and higher polynomials introduced unnecessary complexity and oscillatory behavior without meaningful improvement in predictive performance. Accordingly, a fifth-order polynomial was selected to balance fitting accuracy and model complexity for the present dataset. The final regression equations are presented in Eqs. (1) and (2), with coefficients rounded to six

Table 4
Experimental case classification.

	Range
ΔT	1, 2, 3, 4, 5, 6, 7, 8, 9, 10, 11, 12, 13, 14, 15 °C
Materials	Aluminum, Copper

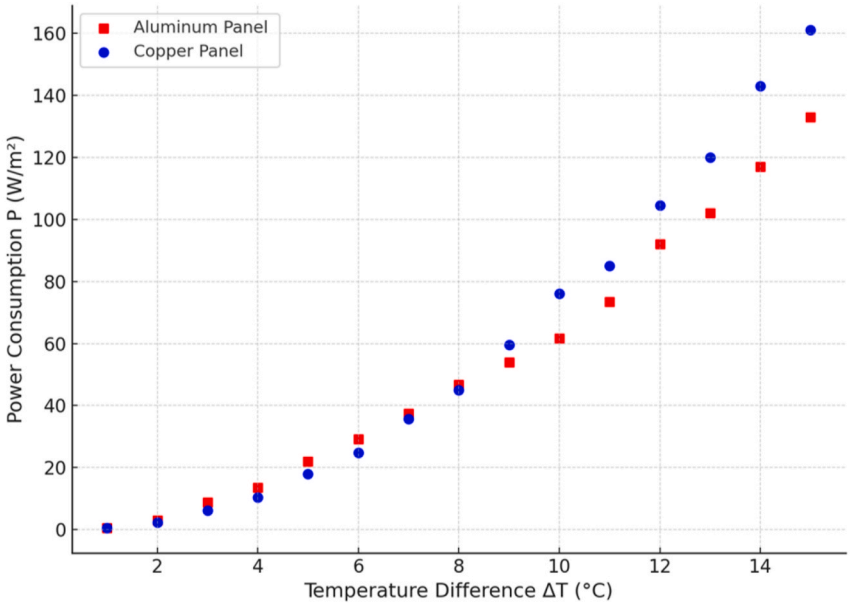

ΔT (℃)	1	2	3	4	5	6	7	8	9	10	11	12	13	14	15
P (W/m²) [Aluminium]	0.5	3.0	8.8	13.5	22.0	29.3	37.5	46.8	54.0	61.8	73.5	92.0	102.0	117.0	133.0
P (W/m²) [Copper]	0.5	2.3	6.3	10.5	18.0	24.8	35.8	45.0	59.5	76.0	85.0	104.5	120.0	143.0	161.0

Fig. 10. Power consumption of thermoelectric panels.

decimal places to ensure reproducibility and practical implementation. The applicability of the regression models is limited to the tested ΔT range of 1–15 °C, the 5 × 5 prototype configuration, the aluminum and copper plate assemblies, and the controlled chamber boundary conditions used in this study. Although this ΔT range covers the expected operating range considered in the present analysis, extrapolation beyond the tested conditions should be avoided without additional validation. The reported fit statistics characterize agreement with the experimental dataset and do not, by themselves, constitute independent validation. A semi-empirical model based

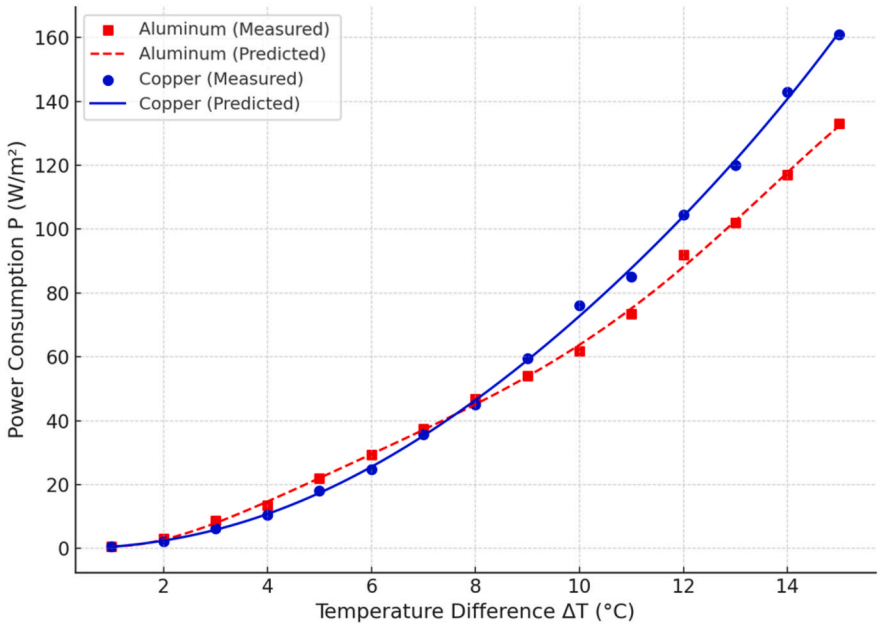

Fig. 11. Measured vs. predicted consumption.

on thermoelectric heat-transfer relations could improve physical interpretability, but would require identification and validation of effective module parameters, interfacial thermal resistances, and assembly heat losses. The present regressions are therefore intended as electrical-input correlations within the stated experimental limits.

Aluminum panel:

$$P = 4.112238 - 7.157083\Delta T + 4.315808\Delta T^2 - 0.617341\Delta T^3 + 0.041839\Delta T^4 - 0.001014\Delta T^5 \quad (1)$$

Copper panel:

$$P = -0.256643 + 0.268652\Delta T + 0.417467\Delta T^2 + 0.073774\Delta T^3 - 0.006248\Delta T^4 + 0.000173\Delta T^5 \quad (2)$$

In these equations, P represents the power consumption in W/m^2, while ΔT denotes the temperature difference between the hot and cold sides in °C. Fig. 11 compares the regression curves with the experimental data and indicates that the models accurately represent power consumption within the tested ΔT range. For the aluminum-based panel, the coefficient of determination (R^2) reached 0.999 and the root mean square error (RMSE) was 1.36 W/m^2. For the copper-based panel, R^2 also reached 0.999 while the RMSE was 1.43 W/m^2. Both regression models therefore showed high predictive accuracy within the tested experimental range, with residuals confined within ±2 W/m^2 as illustrated in Fig. 12. When the models were further evaluated against ±10% error bounds, the data points for both aluminum and copper prototypes were distributed well inside the acceptable region. This outcome supports the reliability of the derived regression equations within the experimental range considered in this study.

The regression models reproduced the measured nonlinear increase in electrical demand and the crossover near 8 °C. This agreement does not independently identify the heat-transfer mechanisms responsible for the material-dependent behavior. Alternative regressions, including quadratic, cubic, and exponential forms, were less successful in representing the measured curvature and steep increase at larger ΔT. The fifth-order polynomial was therefore retained as an empirical representation of the present data.

The correlations may be incorporated into simulation environments such as EnergyPlus and TRNSYS to estimate panel electrical input, provided their experimental limits are respected. They do not constitute a validated wall heat-transfer model or establish whole-building energy savings. Application to other configurations or boundary conditions requires additional validation and, where necessary, recalibration.

4.3. Uncertainty analysis

Following the ASHRAE guidelines [40], an uncertainty analysis was performed to evaluate the reliability and accuracy of the experimental measurements. As shown in Eq. (3), the total uncertainty (*Uy*) comprises two elements: the propagation uncertainty (*By*) and random uncertainty (*Py*). The propagation uncertainty was estimated using a fixed error term (*bxi*), which was calculated by multiplying the standard deviation of the recorded temperature (*Sr*) by the rated accuracy of the thermocouple sensors, as expressed in Eq. (4). The random uncertainty was determined according to Eq. (5) using the statistical relationship between the standard deviation and mean value (*M*) of the dataset. The overall uncertainty in each case was then obtained from the measured parameters (*xi*). The outcomes of this analysis, derived from the validation experiment dataset, are summarized in Table 5 and represent the uncertainty range of the thermoelectric active insulation system.

$$U_y = \sqrt{\left(B_y^2 + P_y^2\right)} \quad (3)$$

$$B_y = \sqrt{\left[\sum_{i=1}^{n}\left(\frac{dy}{dx_i}B_{x_i}\right)^2\right]} \quad (4)$$

$$P_y = \frac{2S_r}{\sqrt{M}} \quad (5)$$

To strengthen the robustness of the analysis, repeated measurements were carried out for every test condition. The resulting data were processed using established statistical methods to minimize potential bias. This procedure ensures that the reported uncertainties reflect both systematic and random sources of error, producing a comprehensive evaluation of measurement reliability. In addition, the framework adopted for uncertainty assessment promotes reproducibility and allows a direct comparison with related thermoelectric system studies in the literature.

5. Conclusions

This study introduced a thermoelectric active insulation concept and experimentally characterized the electrical input required to maintain prescribed temperature differences across prototype panels. The proposed boundary-matching approach is intended to modify heat transfer through opaque walls. The experiments provide prototype-level electrical-input characteristics and empirical correlations, while wall-scale heat-transfer reduction and net building energy savings remain to be verified.

Two prototype panels were fabricated, each containing 25 thermoelectric modules arranged in a 5 × 5 matrix. The modules measured 40 mm × 40 mm and were bonded to metallic plates of 1 mm thickness, which provided structural rigidity and lateral

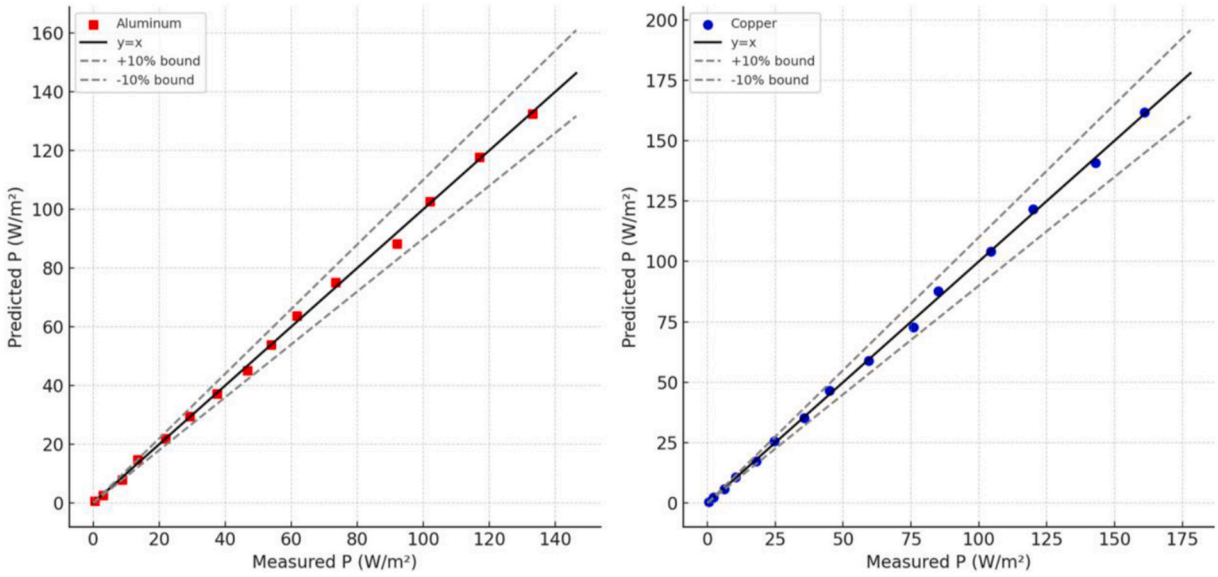

Fig. 12. Residuals of aluminum and copper models.

Table 5
Measurement uncertainty.

ΔT	I	V	P
0.71%	2.16%	0.71%	1.86%

thermal diffusion. The electrical design placed five modules in series and five strings in parallel, thereby satisfying the current and voltage limits specified by the manufacturer while balancing the power distribution. The active measurement area at the core of the array was 200 mm × 200 mm. This design enabled a controlled comparison between aluminum and copper plates while offering a realistic basis for scaling to building-sized assemblies.

The experiments were conducted in a chamber with controlled temperature and humidity. The hot side was maintained within the indoor comfort range, while the cold side was coupled to a constant-temperature surface representing the wall-side boundary. Tests covered $\Delta T = 1$ to 15 °C at 1 °C intervals. Electrical demand was relatively low below approximately 9 °C and increased more rapidly at larger ΔT under the tested conditions; this observation does not establish net energy savings. The aluminum and copper prototypes exhibited a power-consumption crossover near 8 °C, although its underlying mechanisms were not independently resolved. The limited calibration results support using ΔT as the predictor within the present experimental conditions, but do not establish general applicability across climates or absolute temperatures.

Empirical models were developed to predict power demand as a function of ΔT. Fifth-order polynomial regressions represented the measured data for both the aluminum and copper prototypes, with coefficients of determination close to 1 and RMSEs on the order of 1–2 W/m^2. The residuals were small and evenly distributed across the operating range. The models may be used as electrical-input correlations within their stated experimental limits; extension to other conditions requires validation and, where necessary, recalibration. An uncertainty analysis following accepted procedures confirmed low combined uncertainties for temperature, current, voltage, and power, and repeated measurements improved reproducibility.

The broader implications extend to energy efficiency, comfort, and renovation practice. Maintaining interior surfaces near indoor setpoints may reduce radiant asymmetry and cold-wall discomfort, although these effects were not directly evaluated. By keeping surfaces above the dew point, condensation and mold risk may be reduced under suitable operating conditions. As a prefabricated interior layer, the panel can be installed with minimal demolition and without altering facades, providing a practical path for upgrading occupied buildings where conventional retrofits are difficult owing to structural, policy, or cost constraints. Comparatively, the system suggests a thin assembly profile and potential operational flexibility, while avoiding the fluid networks and high maintenance of hydronic or coil-based barriers.

Limitations remain. Electrical demand increases at larger ΔT, while the coefficient of performance and net energy benefit were not determined in the present experiments. Practical performance depends on plate properties, contact quality, joint thermal bridging, and control stability. Repeated thermal cycling and humid exposure may affect joint integrity and electrical and thermal contact properties, making long-term stability a design constraint [41]. Material-specific research on moisture stability further highlights the importance of environmental durability, without establishing the moisture resistance of the present prototype [42]. Moisture management at the concealed wall-facing interface depends on the sealed installation assumption described in Section 2.2 and on wall-specific moisture

conditions. Detailed condensation, frost, and durability assessments were outside the present experimental scope. Cost, installation logistics, and code compliance also require evaluation before practical deployment.

Future research should advance along four directions. First, direct heat-flux measurements and guarded or calibrated hot-box experiments are needed to quantify conductive heat-transfer reduction and apparent changes in effective thermal resistance under controlled wall-assembly conditions. Second, field demonstrations across diverse climates and wall types are needed to validate seasonal performance, boundary conditions, and interactions with ventilation and solar exposure. Third, closed-loop control experiments should be conducted to evaluate transient response, response time, disturbance rejection, and sensor-feedback stability. Fourth, whole-building assessments should consider energy balance, life cycle cost, embodied impact, code compliance, comfort, and maintenance. These steps are necessary to verify the conceptual implications identified in this proof-of-concept study and to advance the technology from laboratory characterization to building-scale application.

In conclusion, the thermoelectric active insulation panel offers a promising proof-of-concept approach for modifying the thermal behavior of opaque walls through electrically imposed boundary matching. Within the tested ΔT range, the experimental results define the electrical power demand of the prototype and provide empirical models suitable for predicting panel power consumption under controlled conditions. The findings suggest potential benefits for conductive heat-transfer suppression, comfort improvement, and retrofit applications. However, direct heat-flux validation, closed energy-balance assessment, and closed-loop control testing are required before confirming whole-building energy savings or fully validated active envelope control performance.

CRediT authorship contribution statement

Minseong Kim: Writing – original draft, Visualization, Validation, Investigation, Data curation. **Junseok Park:** Validation, Software, Methodology. **Jae-Weon Jeong:** Writing – review & editing, Supervision, Project administration, Funding acquisition, Conceptualization.

Funding

This work was supported by the National Research Foundation of Korea (NRF) grant funded by the Korean Government (MSIT) (No. RS-2025-00512834 and No. RS-2025-00518334).

Declaration of competing interest

The authors declare that they have no known competing financial interests or personal relationships that could have appeared to influence the work reported in this paper.

Data availability

Data will be made available on request.

References

[1] F. Ascione, N. Bianco, R.F. De Masi, F. De'Rossi, G.P. Vanoli, Simplified state space representation for evaluating thermal bridges in building: modelling, application and validation of a methodology, Appl. Therm. Eng. 61 (2013) 344–354, https://doi.org/10.1016/j.applthermaleng.2013.07.052.
[2] E. Borri, G. Zsembinszki, L.F. Cabeza, Recent developments of thermal energy storage applications in the built environment: a bibliometric analysis and systematic review, Appl. Therm. Eng. 189 (2021) 116666, https://doi.org/10.1016/j.applthermaleng.2021.116666.
[3] N. Soares, J. Bastos, L.D. Pereira, A. Soares, A.R. Amaral, E. Asadi, E. Rodrigues, F.B. Lamas, H. Monteiro, M.A.R. Lopes, A.R. Gaspar, A review on current advances in the energy and environmental performance of buildings towards a more sustainable built environment, Renew. Sustain. Energy Rev. 77 (2017) 845–860, https://doi.org/10.1016/j.rser.2017.04.027.
[4] J. Alabid, A. Bennadji, M. Seddiki, A review on the energy retrofit policies and improvements of the UK existing buildings, challenges and benefits, Renew. Sustain. Energy Rev. 159 (2022) 112161, https://doi.org/10.1016/j.rser.2022.112161.
[5] S. Abu Dabous, F. Hosny, A review of building envelope retrofitting methods for improving energy efficiency, aesthetic, and indoor environmental quality, Energy Nexus 18 (2025) 100407, https://doi.org/10.1016/j.nexus.2025.100407.
[6] B. Fleury, E. Abraham, J.A. De La Cruz, V.S. Chandrasekar, B. Senyuk, Q. Liu, V. Cherpak, S. Park, J.B. Ten Hove, I.I. Smalyukh, Aerogel from sustainably grown bacterial cellulose pellicles as a thermally insulative film for building envelopes, ACS Appl. Mater. Interfaces 12 (2020) 34115–34121, https://doi.org/10.1021/acsami.0c08879.
[7] L. Shen, Z. Tu, Q. Hu, C. Tao, H. Chen, The optimization design and parametric study of thermoelectric radiant cooling and heating panel, Appl. Therm. Eng. 112 (2017) 688–697, https://doi.org/10.1016/j.applthermaleng.2016.10.094.
[8] C. Shen, X. Li, Dynamic thermal performance of pipe-embedded building envelope utilizing evaporative cooling water in the cooling season, Appl. Therm. Eng. 106 (2016) 1103–1113, https://doi.org/10.1016/j.applthermaleng.2016.06.073.
[9] R.A. Kishore, M.V.A. Bianchi, C. Booten, J. Vidal, R. Jackson, Parametric and sensitivity analysis of a PCM-integrated wall for optimal thermal load modulation in lightweight buildings, Appl. Therm. Eng. 187 (2021) 116568, https://doi.org/10.1016/j.applthermaleng.2021.116568.
[10] M. Saffari, C. Roe, D.P. Finn, Improving the building energy flexibility using PCM-enhanced envelopes, Appl. Therm. Eng. 217 (2022) 119092, https://doi.org/10.1016/j.applthermaleng.2022.119092.
[11] Z. Tian, Y. Liu, Y. Chen, C. Song, Y. Liang, Thermal analysis and optimization of data center building envelope insulation in different climate zones, Appl. Therm. Eng. 257 (2024) 124366, https://doi.org/10.1016/j.applthermaleng.2024.124366.
[12] A. Omidvar, M. Sharifi, Optimizing of thermal insulation thickness in exterior building walls based on adaptive indoor thermostat setpoint strategies in various climatic zones of Iran, Appl. Therm. Eng. 267 (2025) 125830, https://doi.org/10.1016/j.applthermaleng.2025.125830.
[13] H. Lim, Y.K. Kang, J.W. Jeong, Development of empirical models to predict cooling performance of a thermoelectric radiant panel, Energy Build. 202 (2019), https://doi.org/10.1016/j.enbuild.2019.109387.

[14] H. Lim, J.W. Jeong, Energy saving potential of thermoelectric radiant cooling panels with a dedicated outdoor air system, Energy Build. 169 (2018) 353–365, https://doi.org/10.1016/j.enbuild.2018.03.062.
[15] L. Gragnaniello, M. Iasiello, G.M. Mauro, Multi-objective optimization of a heat sink for the thermal management of a peltier-cell-based biomedical refrigerator, Energies 15 (2022), https://doi.org/10.3390/en15197352.
[16] C.H. Lozinsky, N. Casquero-Modrego, I.S. Walker, The health and indoor environmental quality impacts of residential building envelope retrofits: a literature review, Build. Environ. 270 (2025) 112568, https://doi.org/10.1016/j.buildenv.2025.112568.
[17] M. Ozel, Thermal performance and optimum insulation thickness of building walls with different structure materials, Appl. Therm. Eng. 31 (2011) 3854–3863, https://doi.org/10.1016/j.applthermaleng.2011.07.033.
[18] A. Bolattürk, Determination of optimum insulation thickness for building walls with respect to various fuels and climate zones in Turkey, Appl. Therm. Eng. 26 (2006) 1301–1309, https://doi.org/10.1016/j.applthermaleng.2005.10.019.
[19] M. Kayfeci, A. Keçebaş, E. Gedik, Determination of optimum insulation thickness of external walls with two different methods in cooling applications, Appl. Therm. Eng. 50 (2013) 217–224, https://doi.org/10.1016/j.applthermaleng.2012.06.031.
[20] M. Khoukhi, N. Fezzioui, B. Draoui, L. Salah, The impact of changes in thermal conductivity of polystyrene insulation material under different operating temperatures on the heat transfer through the building envelope, Appl. Therm. Eng. 105 (2016) 669–674, https://doi.org/10.1016/j.applthermaleng.2016.03.065.
[21] S. Mao, A. Kan, N. Wang, Numerical analysis and experimental investigation on thermal bridge effect of vacuum insulation panel, Appl. Therm. Eng. 169 (2020) 114980, https://doi.org/10.1016/j.applthermaleng.2020.114980.
[22] F. Aguilar, J.P. Solano, P.G. Vicente, Transient modeling of high-inertial thermal bridges in buildings using the equivalent thermal wall method, Appl. Therm. Eng. 67 (2014) 370–377, https://doi.org/10.1016/j.applthermaleng.2014.03.058.
[23] A.P. Gomes, H.A. De Souza, A. Tribess, Impact of thermal bridging on the performance of buildings using light steel framing in Brazil, Appl. Therm. Eng. 52 (2013) 84–89, https://doi.org/10.1016/j.applthermaleng.2012.11.015.
[24] M. De Rosa, V. Bianco, F. Scarpa, L.A. Tagliafico, Heating and cooling building energy demand evaluation; A simplified model and a modified degree days approach, Appl. Energy 128 (2014) 217–229, https://doi.org/10.1016/j.apenergy.2014.04.067.
[25] Y. Luo, L. Zhang, Z. Liu, J. Wu, Y. Zhang, Z. Wu, Numerical evaluation on energy saving potential of a solar photovoltaic thermoelectric radiant wall system in cooling dominant climates, Energy 142 (2018) 384–399, https://doi.org/10.1016/j.energy.2017.10.050.
[26] Y. Luo, L. Zhang, Z. Liu, J. Wu, Y. Zhang, Z. Wu, Three dimensional temperature field of thermoelectric radiant panel system: analytical modeling and experimental validation, Int. J. Heat Mass Tran. 114 (2017) 169–186, https://doi.org/10.1016/j.ijheatmasstransfer.2017.06.063.
[27] R.M. Atta, Solar water condensation using thermoelectric coolers, Int. J. Adv. Eng. Res. Dev. 4 (2017), https://doi.org/10.21090/ijaerd.96616.
[28] A. Karanafti, T. Theodosiou, K. Tsikaloudaki, Assessment of buildings' dynamic thermal insulation technologies-A review, Appl. Energy 326 (2022) 119985, https://doi.org/10.1016/j.apenergy.2022.119985.
[29] D.H.W. Li, L. Yang, J.C. Lam, Zero energy buildings and sustainable development implications - a review, Energy 54 (2013) 1–10, https://doi.org/10.1016/j.energy.2013.01.070.
[30] H.M. Künzel, A. Holm, D. Zirkelbach, A.N. Karagiozis, Simulation of indoor temperature and humidity conditions including hygrothermal interactions with the building envelope, Sol. Energy 78 (2005) 554–561, https://doi.org/10.1016/j.solener.2004.03.002.
[31] U.S. Environmental Protection Agency, Moisture control guidance for building design , construction and maintenance, Indoor Air Qual. Div (2013) 144. https://www.epa.gov/iaq/moisture.
[32] Y. Xue, Y. Fan, Z. Wang, W. Gao, Z. Sun, J. Ge, Facilitator of moisture accumulation in building envelopes and its influences on condensation and mould growth, Energy Build. 277 (2022) 112528, https://doi.org/10.1016/j.enbuild.2022.112528.
[33] N. Al-Tamimi, Building envelope retrofitting strategies for energy-efficient office buildings in Saudi Arabia, Buildings 12 (2022), https://doi.org/10.3390/buildings12111900.
[34] S. Liu, F.E.M. Ghazali, J. Yang, Z. Guo, K. Zeng, Y. Chen, Retrofit analysis of exterior windows for large office buildings in different climate zones of China, Buildings 14 (2024), https://doi.org/10.3390/buildings14123904.
[35] D. Astrain, J.G. Vián, M. Domínguez, Increase of COP in the thermoelectric refrigeration by the optimization of heat dissipation, Appl. Therm. Eng. 23 (2003) 2183–2200, https://doi.org/10.1016/S1359-4311(03)00202-3.
[36] ANSI/ASHRAE Standard 55-2013 : Thermal Environmental Conditions for Human Occupancy, 2022, 2022.
[37] M. Kim, Y.K. Kang, J. Joung, J.W. Jeong, Cooling performance prediction for hydraulic thermoelectric radiant cooling panels with experimental validation, Sustain 14 (2022), https://doi.org/10.3390/su142316214.
[38] I.T. Hebei, Performance specifications of TEC1-12706, Appl. Note (2010) 2–4. https://peltiermodules.com/peltier.datasheet/TEC1-12706.pdf.
[39] M. Kim, J.W. Jeong, Applicability analysis of thermoelectric active condensation prevention system in buildings, Energy Build. 347 (2025) 116309, https://doi.org/10.1016/j.enbuild.2025.116309.
[40] ASHARE, ASHRAE Guideline 2-2010 Engineering Analysis of Experimental Data, ASHRAE Guidel, 2010, p. 2010.
[41] X. Wu, T. Mori, W. Liu, Thermoelectric stability as a design constraint for energy conversion, Joule 10 (2026) 102421, https://doi.org/10.1016/j.joule.2026.102421.
[42] X. Wu, L. Wang, G. Wu, A. Li, T. Mori, Moisture-stable Mg3(Bi, Sb)2 thermoelectrics enabled by anodic protection, Natl. Sci. Rev. 13 (10) (2026) nwag232, https://doi.org/10.1093/nsr/nwag232.